Study of the decay $\phi \to \pi^+\pi^-\pi^0$ with the KLOE detector.

The KLOE Collaboration

A. Aloisio [e], F. Ambrosino [e], A. Antonelli [b], M. Antonelli [b],
C. Bacci [j], F. Bellini [j], G. Bencivenni [b], S. Bertolucci [b],
C. Bini [h,1], C. Bloise [b], V. Bocci [h], F. Bossi [b], P. Branchini [j],
S. A. Bulychjov [o], G. Cabibbo [h], R. Caloi [h], P. Campana [b],
G. Capon [b], T. Capussela [e], G. Carboni [i], M. Casarsa [ℓ],
V. Casavola [d], G. Cataldi [d], F. Ceradini [j], F. Cervelli [f],
F. Cevenini [e], G. Chiefari [e], P. Ciambrone [b], S. Conetti [m],
E. De Lucia [h], G. De Robertis [a], P. De Simone [b], G. De Zorzi [h],
S. Dell'Agnello [b], A. Denig [c], A. Di Domenico [h], C. Di Donato [e],
S. Di Falco [f], B. Di Micco [j], A. Doria [e], M. Dreucci [b],
O. Erriquez [a], A. Farilla [j], G. Felici [b], A. Ferrari [j], M. L. Ferrer [b],
G. Finocchiaro [b], C. Forti [b], A. Franceschi [b], P. Franzini [h],
C. Gatti [h], P. Gauzzi [h], S. Giovannella [b], E. Gorini [d],
F. Grancagnolo [d], E. Graziani [j], S. W. Han [b,n], M. Incagli [f],
L. Ingrosso [b], W. Kluge [c], C. Kuo [c], V. Kulikov [o], F. Lacava [h],
G. Lanfranchi [b], J. Lee-Franzini [b,k], D. Leone [h], F. Lu [b,n]
M. Martemianov [b], M. Matsyuk [b], W. Mei [b], L. Merola [e],
R. Messi [i], S. Miscetti [b], M. Moulson [b], S. Müller [c], F. Murtas [b],
M. Napolitano [e], A. Nedosekin [b,o], F. Nguyen [j], M. Palutan [b],
E. Pasqualucci [h], L. Passalacqua [b], A. Passeri [j], V. Patera [b,g],
F. Perfetto [e], E. Petrolo [h], G. Pirozzi [e], L. Pontecorvo [h],
M. Primavera [d], F. Ruggieri [a], P. Santangelo [b], E. Santovetti [i],
G. Saracino [e], R. D. Schamberger [k], B. Sciascia [b], A. Sciubba [b,g],
F. Scuri [f], I. Sfiligoi [b], A. Sibidanov [b], P. Silano [h], T. Spadaro [b],
E. Spiriti [j], G. L. Tong [b,n], L. Tortora [j], E. Valente [h],
P. Valente [b], B. Valeriani [c], G. Venanzoni [f], S. Veneziano [h],

---

[1] Corresponding author: Cesare Bini, e-mail cesare.bini@roma1.infn.it, tel +390649914266, fax +39064957697

A. Ventura [d], S.Ventura [h], R.Versaci [j], Y. Xu [b,n], G. W. Yu [b,n]

[a]*Dipartimento di Fisica dell'Università e Sezione INFN, Bari, Italy.*

[b]*Laboratori Nazionali di Frascati dell'INFN, Frascati, Italy.*

[c]*Institut für Experimentelle Kernphysik, Universität Karlsruhe, Germany.*

[d]*Dipartimento di Fisica dell'Università e Sezione INFN, Lecce, Italy.*

[e]*Dipartimento di Scienze Fisiche dell'Università "Federico II" e Sezione INFN, Napoli, Italy*

[f]*Dipartimento di Fisica dell'Università e Sezione INFN, Pisa, Italy.*

[g]*Dipartimento di Energetica dell'Università "La Sapienza", Roma, Italy.*

[h]*Dipartimento di Fisica dell'Università "La Sapienza" e Sezione INFN, Roma, Italy.*

[i]*Dipartimento di Fisica dell'Università "Tor Vergata" e Sezione INFN, Roma, Italy.*

[j]*Dipartimento di Fisica dell'Università "Roma Tre" e Sezione INFN, Roma, Italy.*

[k]*Physics Department, State University of New York at Stony Brook, USA.*

[ℓ]*Dipartimento di Fisica dell'Università e Sezione INFN, Trieste, Italy.*

[m]*Physics Department, University of Virginia, USA.*

[n]*Permanent address: Institute of High Energy Physics, CAS, Beijing, China.*

[o]*Permanent address: Institute for Theoretical and Experimental Physics, Moscow, Russia.*

Abstract

We present a study of the reaction $e^+e^- \to \pi^+\pi^-\pi^0$ at the ϕ peak, $W = M(\phi)$ =1019.4 MeV, observed with the KLOE detector at DAΦNE. The reaction is dominated by ϕ production and decay, $e^+e^- \to \phi \to \pi^+\pi^-\pi^0$. From a fit to the Dalitz plot density distribution we obtain the ρ-meson parameters for its three charge states. We also find the relative amplitudes for $\phi \to \rho\pi$ and $\phi \to \pi^+\pi^-\pi^0$ and the cross section for $e^+e^- \to \omega\pi^0$ with $\omega \to \pi^+\pi^-$.

Key words: e^+e^- collisions, $\phi \to \pi^+\pi^-\pi^0$, ρ meson masses and widths
PACS: 13.65.+i, 14.40.Cs

The decay of the ϕ meson to $\pi^+\pi^-\pi^0$, with a branching ratio (BR) of $\sim$15.5%, is dominated by the $\rho\pi$ intermediate states [1] $\rho^+\pi^-$, $\rho^-\pi^+$, and $\rho^0\pi^0$ with equal amplitudes. We use data from $e^+e^- \to \pi^+\pi^-\pi^0$ to determine the masses and widths of the three charge states of the ρ-meson. CPT invariance requires equality of the masses and widths of ρ^+ and ρ^-, while possible mass or width differences between ρ^0 and $\rho^\pm$ are related to isospin-violating electromagnetic effects. Additional contributions to $e^+e^- \to \pi^+\pi^-\pi^0$ are the so called "direct term", $\phi \to \pi^+\pi^-\pi^0$[2], and $e^+e^- \to \omega\pi^0$, $\omega \to \pi^+\pi^-$.

We define the variables $x = T^+ - T^-$ and $y = T^0$, where $T^{+,-,0}$ are the kinetic energies of the three pions in the center of mass system (CM). The Dalitz plot density distribution $D(x,y)$, in terms of the three amplitudes is given by:

$$D(x,y) \propto |\vec{p}_+^* \times \vec{p}_-^*|^2 |A_{\rho\pi} + A_{\mathrm{dir}} + A_{\omega\pi}|^2 \qquad (1)$$

where $\vec{p}_\pm^*$ are the $\pi^\pm$ momenta in the CM and $A_{\rho\pi}$, A_{dir} and $A_{\omega\pi}$ are the amplitudes described above.

Some 2 million $\pi^+\pi^-\pi^0$ events were collected with the KLOE detector in e^+e^- collisions at the Frascati ϕ-factory DAΦNE, in the fall of 2000. DAΦNE was run at a CM energy $W = M(\phi)$ and the integrated luminosity was Ł=16 pb^{-1}. In the following we present an analysis of the Dalitz plot density distribution and new determinations of $\Gamma(\rho^{+-0})$, $M(\rho^{+-0})$, $A_{\rho\pi}$, A_{dir}, $A_{\omega\pi}$ and $\sigma(e^+e^- \to \omega\pi^0, \omega \to \pi^+\pi^-)$ at $W = 1019.4$ MeV.

The KLOE detector consists of a large volume drift chamber [3] (3.3 m length and 2 m radius), operated with a 90% helium-10% isobutane gas mixture, and a sampling electromagnetic calorimeter [4] made of lead and scintillating fibres. The whole detector is surrounded by a superconducting coil producing a solenoidal field B=0.52 T. The drift chamber momentum resolution is $\sigma(p_\perp)/p_\perp \sim 0.4\%$. The calorimeter determines photon impact points to an accuracy of 1 cm $/\sqrt{E(\mathrm{GeV})}$ in the direction along the fibres and of 1 cm in the transverse direction. Photon energies and arrival times are measured with resolutions of $\sigma(E)/E = 5.7\%/\sqrt{E(\mathrm{GeV})}$ and $\sigma(t) = 57\mathrm{ps}/\sqrt{E(\mathrm{GeV})} \oplus 50$ ps. The solid angle coverage of the calorimeter is 98% of 4π; however particles from the interaction point with a polar angle with respect to the beam axis $\theta < 15°$ are shadowed by the low-β insertion quadrupoles. The trigger [5] is based on the coincidence of at least two local energy deposits in the calorimeter, above a threshold that ranges between 50 and 150 MeV. In order to reduce the trigger rate due to cosmic rays crossing the detector, events with a large energy release in the outermost calorimeter planes are vetoed.

The DAΦNE beams collide with a crossing angle of 25 mrad, so the ϕ is produced with a momentum in the horizontal plane $|\vec{p}_\phi| \sim 12.5$ MeV. $\pi^+\pi^-\pi^0$ events are selected by asking for two non-collinear tracks with opposite sign of curvature and polar angle $\theta > 40°$ which intersect the interaction region. The acollinearity cut ($\Delta\theta < 175°$) removes $e^+e^-\gamma$ events without incurring an acceptance loss for the signal. We then compute the missing mass, $M_{\mathrm{miss}} = \sqrt{(E_\phi - E_{\pi^+} - E_{\pi^-})^2 - |\vec{p}_\phi - \vec{p}_{\pi^+} - \vec{p}_{\pi^-}|^2}$ where E and $\vec{p}$ are laboratory energies and momenta. M_{miss} is required to be within 20 MeV of the π^0 mass. This requirement corresponds to an effective energy cut of ≤ 20 MeV on the total energy radiated because of initial state radiation (ISR). Two photons
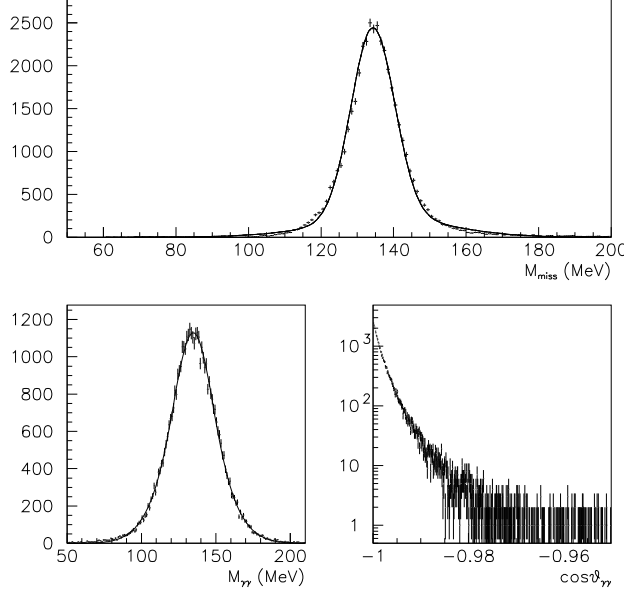
Fig. 1. Distributions of M_{miss} (top), $M_{\gamma\gamma}$, and $\cos\theta_{\gamma\gamma}$ (bottom left and right) for a sample of selected events. The rms widths of the M_{miss} and $M_{\gamma\gamma}$ distributions are 5.5 MeV and 17 MeV, respectively. The solid lines are gaussian fits.

in the calorimeter are also required. A photon is defined as an energy deposit larger than 10 MeV with $21° < \theta < 159°$ and an arrival time compatible with a particle travelling at the speed of light, within $5\sigma(t)$. The two-photon opening angle in the π^0 rest frame must satisfy $\cos\theta_{\gamma\gamma} < -0.98$.

Fig. 1 shows the distributions of the missing mass M_{miss}, of the $\gamma\gamma$ invariant mass, and of $\cos\theta_{\gamma\gamma}$ for a sample of selected events. Due to the large cross-section [2] for this final state with respect to other processes ($\sigma_\phi \times \mathrm{BR}(\phi \to \pi^+\pi^-\pi^0) = 460$ nb) and to the clean signature, the background to this process after the selection described is $\leq 10^{-5}$. The Dalitz plot variables x and y are evaluated using the measured momenta of the charged pions, boosted to the center of mass system: $x = E_+^* - E_-^*$ and $y = E_\phi^* - E_+^* - E_-^* - M_{\pi^0} = T_{\pi^0}$. E_ϕ and $\vec{p}_\phi$ are measured run by run using Bhabha scattering events. ISR lowers the mean $\pi^+\pi^-\pi^0$ total energy by $\sim$130 keV. This value is used in the analysis with negligible effect on the results. The resolution on x and y is about 1 MeV over the full kinematical range.

The Dalitz plot density distribution is shown in Fig. 2. In the plot the number of events corrected for the efficiency is shown divided by $|\vec{p}_+^* \times \vec{p}_-^*|^2$. Three bands corresponding to the three ρ states are clearly evident. The two-

---

[2] Here and in the following we consider visible cross-sections, not corrected for the effect of the radiative corrections.
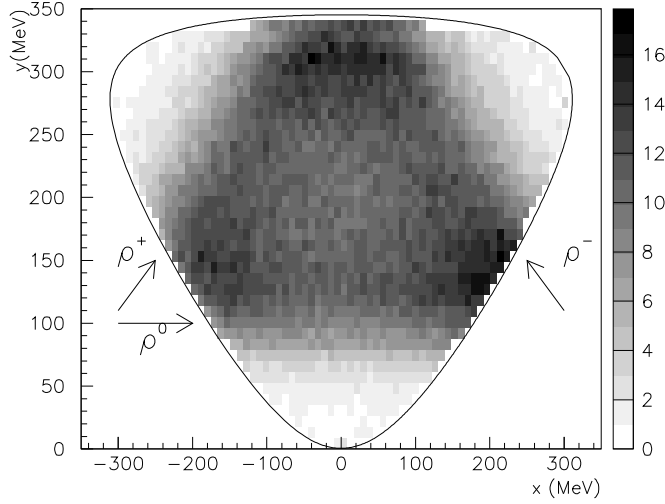
Fig. 2. Distribution of the number of events corrected for the efficiency and divided by $|\vec{p}_+^* \times \vec{p}_-^*|^2$. The grey scale is in arbitrary units. The plot contains 1.98 millions events in 1874 bins 8.75×8.75 MeV^2 each. Three broad bands corresponding to the three ρ states are indicated. The kinematical boundary is also shown.

dimensional distribution is plotted in 8.75×8.75 MeV^2 bins. There are 1874 bins within the kinematic boundary. The bin width is larger than the x and y resolution, but is small compared to the density variations of the Dalitz plot as can be seen in the x and y projections shown in Fig. 3. Smearing effects due to the resolution are negligible.

Trigger and selection efficiencies have been evaluated as functions of x and y. A full Monte Carlo simulation of the detector has been used with corrections based on control samples of data. Corrections to the detection efficiency for low energy photons have been obtained using $e^+e^-\gamma$ events while analysis of tracking efficiency shows that the ratio of data to Monte Carlo efficiency is very close to 1 and uniform in the relevant momentum range. The trigger cosmic ray veto rejects ∼5% of the $\pi^+\pi^-\pi^0$ events. The amount and the distribution of the rejected events in the Dalitz plot has been evaluated using downscaled samples of vetoed events. Fig. 4 shows the efficiency bin by bin obtained from a sample of 5×10^6 Monte Carlo events. It can be noticed that the overall efficiency ranges between 20% and 30% within the Dalitz plot. The efficiency is dominated by acceptance cuts on charged tracks and photons. In particular, the low efficiency in the upper corners is due to the fact that low momentum pions do not reach the drift chamber. The uncertainty on the efficiency is dominated by Monte Carlo statistics and is on the order of 1% in each bin.

The calibration of the momentum scale is checked using the measured missing mass M_{miss}. The central value of M_{miss} differs from M_{π^0} by less than 0.1 MeV.
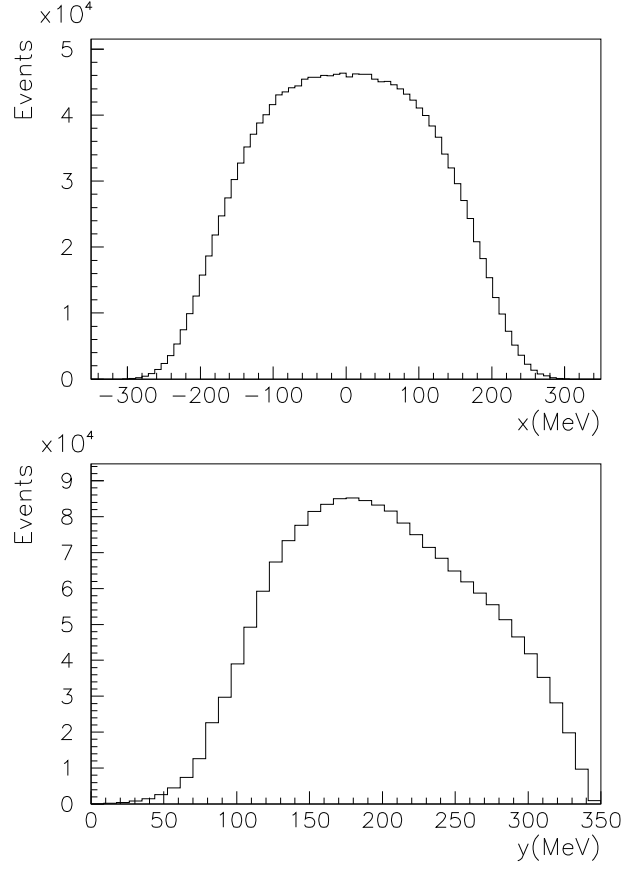
6

Fig. 3. Distributions in x and y of the number of events. The ω peak is not visible because of the smallness of the signal.

The rms fluctuation of the missing mass across the entire Dalitz plot is 0.25 MeV. The latter value is used in the estimates of systematic uncertainties for masses and widths.

The Dalitz plot distribution has been fitted according to Eq. 1. The $\rho\pi$ term includes the line-shape of the three charge states of the ρ [6,7,8] :

$$A_{\rho\pi} = a_\rho \Sigma_k \frac{M_k^2}{q_k^2 - M_k^2 + iq_k \Gamma_{(k)}(q_k^2)} \tag{2}$$

where $k = +, -, 0$ is the ρ-meson charge and $\Gamma_{(k)}(q_k^2)$ is defined as:

$$\Gamma_{(k)}(q_k^2) = \Gamma_k \left(\frac{p_\pi(q_k^2)}{p_\pi(M_k^2)} \right)^3 \left(\frac{M_k^2}{q_k^2} \right) \tag{3}$$

In the above, q_k^2 is the invariant mass of the appropriate pion pair, $\pi^i \pi^j$ with $i, j, k = +, -, 0$; M_k is the ρ mass; Γ_k the width; and p_π is the pion momentum
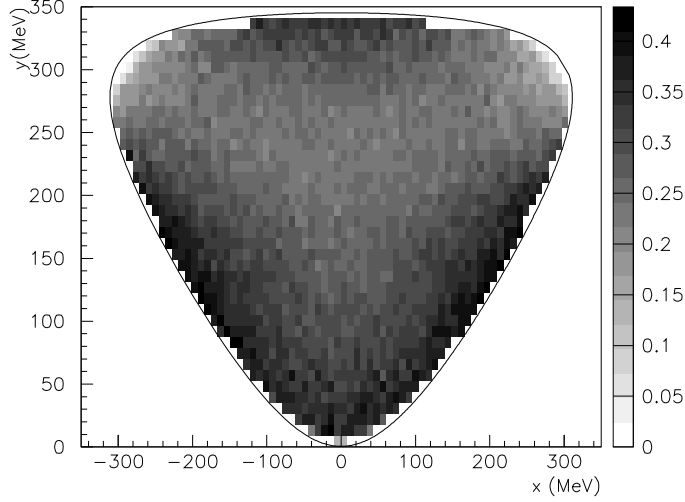
7

Fig. 4. Overall trigger and selection efficiency including the applied corrections as a function of the position in the Dalitz plot.

in the ρ center of mass. The direct amplitude does not in general have the same phase as $A_{\rho\pi}$ and is taken as $A_{\mathrm{dir}} = a_d e^{i\phi_d}$. This term can be interpreted as the sum of ρ-like resonances of higher mass like $\phi \to \rho'(1415)\pi$, which is not distinguishable from a constant term multiplied by $\times |\vec{p}_+^* \times \vec{p}_-^*|^2$. The $\omega\pi$ term is restricted to a horizontal band around $y = 83.7$ MeV, the kinetic energy of the π^0 in the $\omega\pi^0$ final state. The amplitude is given by:

$$A_{\omega\pi} = a_\omega e^{i\phi_\omega} \frac{M_\omega^2}{q_0^2 - M_\omega^2 + i q_0 \Gamma_\omega} \tag{4}$$

with the ω parameters fixed to PDG values [9]. a_ρ, a_ω and a_d are three dimensionless parameters.

We perform a χ^2 fit of the described density function to the data binned as described. The errors used are from data statistics and Monte Carlo statistics for efficiency calculations. Three fits have been performed: a) a fit assuming CPT and isospin invariance, *i.e.* $M_{\rho^0} = M_{\rho^+} = M_{\rho^-}$, $\Gamma_{\rho^0} = \Gamma_{\rho^+} = \Gamma_{\rho^-}$; b) a fit assuming only CPT invariance *i.e.* $M_{\rho^+} = M_{\rho^-}$, $\Gamma_{\rho^+} = \Gamma_{\rho^-}$; and finally c) without limitations on masses and widths. Moduli and phases of direct and $\omega\pi$ terms and a_ρ are also free parameters. There are 7 free parameters for fit a), 9 for fit b) and 11 for fit c). The number of degrees of freedom is 1874−7=1867 for fit a), 1865 for fit b) and 1863 for fit c). The results of the fits are shown in Tab. 1 and a one-dimensional comparison of the data with the fit function (fit (c)) is shown in Fig. 5.

The uncertainties on the parameters are given as the sum of fit uncertainties
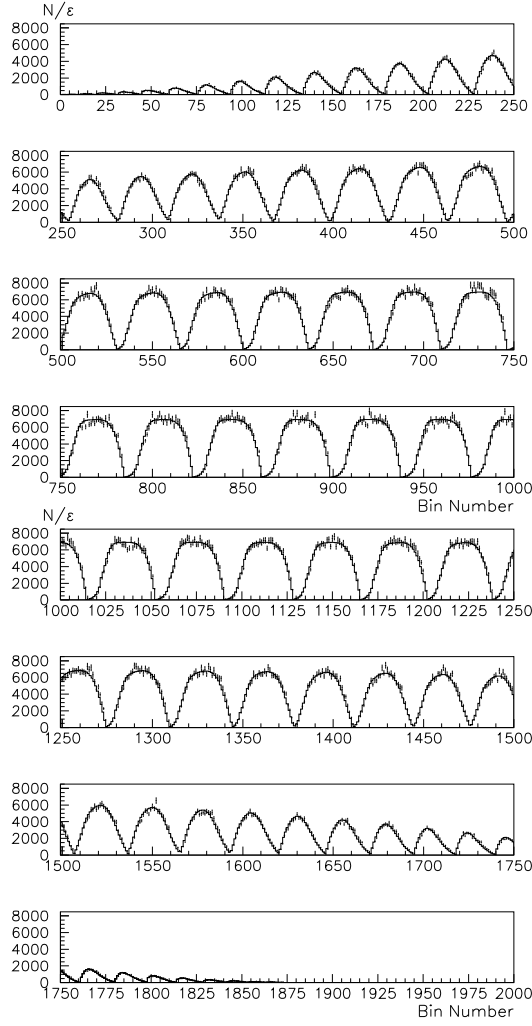
8

Fig. 5. Comparison between efficiency corrected data (points, N/ϵ is number of events per bin divided by the bin efficiency) and fitted function (histogram) as a function of the bin number. The structure observed is due to the y distributions for x slices.

(due to event statistics and efficiencies) and systematic uncertainties coming from two sources: (a) the stability of the fit with respect to changes of the selection cuts, and (b) the absolute momentum calibration. Source (a) is dominant, and is evaluated by repeating the fit for data samples obtained using different values of the cuts and taking the rms variation of the parameters. Effects due to the modelling of ISR are automatically taken into account by the variation of the cut on the missing mass.

Fit (a) converges to an acceptable χ^2 probability, showing that the experimental distribution is consistent with CPT and isospin invariance. Mass and width differences between states of charge obtained by fit (b) and fit (c) are summarized in Tab. 2 where $M_{\rho^\pm} = (M_{\rho^+} + M_{\rho^-})/2$ and $\Gamma_{\rho^\pm} = (\Gamma_{\rho^+} + \Gamma_{\rho^-})/2$.

9

Table 1
Fit results. Masses and widths are in MeV. The amplitudes are scaled in such a way that $a_\rho = 1$. ϕ_d and ϕ_ω are in radians. χ^2 values and probabilities of the fits are given in the first row.

parameter	fit(a)	fit(b)	fit(c)
$\chi^2 \ [p(\chi^2)]$	1939 [12%]	1914 [21%]	1902 [26%]
M_{ρ^0}		$775.9 \pm 0.5 \pm 0.5$	$775.9 \pm 0.6 \pm 0.5$
M_{ρ^+}	$775.8 \pm 0.5 \pm 0.3$	$775.5 \pm 0.5 \pm 0.4$	$776.3 \pm 0.6 \pm 0.7$
M_{ρ^-}			$774.8 \pm 0.6 \pm 0.4$
Γ_{ρ^0}		$147.3 \pm 1.5 \pm 0.7$	$147.4 \pm 1.5 \pm 0.7$
Γ_{ρ^+}	$143.9 \pm 1.3 \pm 1.1$	$143.7 \pm 1.3 \pm 1.2$	$144.7 \pm 1.4 \pm 1.2$
Γ_{ρ^-}			$142.9 \pm 1.3 \pm 1.4$
a_d	$0.78 \pm 0.09 \pm 0.13$	$0.72 \pm 0.09 \pm 0.05$	$0.71 \pm 0.09 \pm 0.05$
ϕ_d	$-2.47 \pm 0.08 \pm 0.08$	$-2.43 \pm 0.10 \pm 0.08$	$-2.43 \pm 0.10 \pm 0.08$
$a_\omega \times 10^3$	$7.1 \pm 0.6 \pm 0.8$	$9.0 \pm 0.7 \pm 0.7$	$9.0 \pm 0.7 \pm 0.3$
ϕ_ω	$-0.22 \pm 0.11 \pm 0.04$	$-0.10 \pm 0.10 \pm 0.05$	$-0.10 \pm 0.10 \pm 0.07$

The ρ masses are significantly larger and the widths smaller than the PDG averages ($M_\rho = 771.1 \pm 0.9$ MeV and $\Gamma_\rho = 149.2 \pm 0.7$ MeV, see [9]) but are close to recent results [10,11,12] for the ρ^0 mass and width.

Table 2
Mass and width differences (in MeV) between ρ-mesons, from fit (b) and fit (c). Errors include the correlations between parameters.

$M_{\rho^0} - M_{\rho^\pm}$	$0.4 \pm 0.7 \pm 0.6$
$M_{\rho^+} - M_{\rho^-}$	$1.5 \pm 0.8 \pm 0.7$
$\Gamma_{\rho^0} - \Gamma_{\rho^\pm}$	$3.6 \pm 1.8 \pm 1.7$
$\Gamma_{\rho^+} - \Gamma_{\rho^-}$	$1.8 \pm 2.0 \pm 0.5$

We observe significant contributions from the direct term and from the $\omega\pi$ term: the coefficients a_d and a_ω are significantly different from 0. If we define the weight of each contribution α ($\alpha = \rho\pi$, dir and $\omega\pi$) as $I_\alpha = \int dx dy |A_\alpha|^2 / \int dx dy |A_{\text{tot}}|^2$, where the amplitudes A_α are taken from the results of fit c) and A_{tot} is the sum of three amplitudes, we get the following weights:

$$I_{\rho\pi} = 0.937 \tag{5}$$

$$I_{\text{dir}} = 8.5 \times 10^{-3} \tag{6}$$

$$I_{\omega\pi} = 2.0 \times 10^{-4} \tag{7}$$

The sum of the three weights is not equal to one, due to a sizeable interference term between $A_{\rho\pi}$ and $A_{\rm dir}$ accounting for about 6% of the total.

From $I_{\omega\pi}$, if we neglect interference, we obtain the visible cross section for the non resonant process $e^+e^- \to \omega\pi^0$ with $\omega \to \pi^+\pi^-$ at $W = 1019.4$ MeV.

$$\sigma(e^+e^- \to \omega\pi^0 \to \pi^+\pi^-\pi^0) = I_{\omega\pi} \times \sigma(e^+e^- \to \pi^+\pi^-\pi^0) = 92 \pm 15 \text{ pb} \tag{8}$$

The ratio of this cross-section to the value $\sigma(e^+e^- \to \omega\pi^0 \to \pi^0\pi^0\gamma) = 0.46 \pm 0.01 \pm 0.03$ nb obtained by KLOE in the 5 photons analysis [13] gives:

$$R = \frac{{\rm BR}(\omega \to \pi^+\pi^-)}{{\rm BR}(\omega \to \pi^0\gamma)} = 0.20 \pm 0.04 \tag{9}$$

which compares well with the value 1.7/8.7=0.20±0.03 from [9].

Acknowledgements

References

[1] A. London et al., Phys. Rev. **143** 1034 (1966);
     G. Cosme et al., Phys. Lett. **48B** 155 (1974);
     G. Parrour et al., Phys. Lett. **B63** 357 (1976).

[2] S. Rudaz, Phys. Lett. **B145** 281 (1984);
     O. Kaymackalan et al., Phys.Rev. **D30** 594 (1984);
     T. Fujiwara et al., Progr. of Theor. Phys. **73** 926 (1985).

[3] M. Adinolfi et al., KLOE coll., Nucl. Instr. and Meth. **A488** 1 (2002).

[4] M. Adinolfi et al., KLOE coll., Nucl. Instr. and Meth. **A482** 364 (2002).

[5] M. Adinolfi et al., KLOE coll., Nucl. Instr. and Meth. **A492** 134 (2002).

[6] G. Gounaris J.J. Sakurai, Phys. Rev. Lett. **21** 244 (1968).

[7] M. Benayoun et al., Eur. Phys. J. **C2** 269 (1998).

[8] J.H. Kühn and A. Santamaria, Zeit. Phys. **C48** 445 (1990).

[9] K. Hagiwara et al. (PDG), Phys.Rev. **D66**, 010001 (2002).

[10] R. Barate et al., Zeit. Phys. **C76** 15 (1997).

[11] R.R. Akhmetshin et al., Phys. Lett. **B527** 161 (2002).

[12] M.N. Achasov et al., Phys. Rev. **D65** 03002 (2002).

[13] A. Aloisio et al., KLOE coll., Phys. Lett. **B537** 21 (2002).